Exploiting covalent, H-bonding and π-π interactions to design antibacterial PDMS interfaces that load and release salicylic acid.

Ioritz Sorzabal-Bellido[1], Yuri A. Diaz-Fernandez[1], Arturo Susarrey-Arce[1], Adam A. Skelton[3], Fiona McBride[1], Alison J. Beckett[2], Ian A. Prior[2], and Rasmita Raval[1]**

Affiliations:

[1]Open Innovation Hub for Antimicrobial Surfaces, Surface Science Research Centre, Department of Chemistry, University of Liverpool, L69 3BX, UK, and National Biofilm Innovation Centre
Corresponding author e-mails: *raval@liverpool.ac.uk, *yuridiaz@liverpool.ac.uk

[2]Biomedical EM Unit, University of Liverpool, L69 3BX, UK

[3]Department of Chemistry, University of Liverpool, L69 3BX, UK

Keywords: antimicrobial surfaces, post-modified PDMS, salicylic acid, APTES, IPTES, medical device materials

Abstract: Smart antimicrobial surfaces are a powerful tool to prevent bacterial colonisation at surfaces. In this work, we report a successful strategy for the functionalisation of polydimethylsiloxane (PDMS) surfaces, widely used in medical devices, with salicylic acid (SA), a biocide approved for use in humans. Antimicrobial PDMS surfaces were fabricated via a rational design in which bi-functional silane linker molecules were covalently grafted onto the PDMS via one end, while generating soft intermolecular interactions with SA at the other end to enable reversible load-release of the biocide. A molecular level understanding of the interface was obtained using ATR-FTIR, Raman and X-ray Photoelectron spectroscopies, alongside Density Functional Theory. These reveal that the linker molecules dock the SA molecules at the surface via a 1:1 complexation interaction. Furthermore, each 1:1 complex acts as a nucleation point onto which multiple stacks of the biocide are subsequently stabilised via a combination of H-bonding and π-π stacking interactions, thus significantly enhancing SA uptake at the interface. The use of soft H-bonding and π–π interactions to create a reservoir of SA molecules at the PDMS surface is also inherently important in enabling the subsequent release of SA from the interface in order to deliver the antimicrobial effect. The antimicrobial activity of these surfaces against model Gram-positive and Gram-negative bacteria represented by *E. coli*, *S. aureus* and *S. epidermidis* is demonstrated by a log 6 reduction of planktonic bacterial populations and an efficient anti-biofilm activity at the surface.

1. Introduction

Bacterial infections on medical devices account for 60-70% of hospital acquired infections worldwide,[1] having a critical impact on the use of antibiotics and on the emergence of antimicrobial resistance.[2] After initial colonisation of surfaces, bacterial communities undergo changes in metabolic activity that may lead to the formation of multicellular structures known as biofilms.[3,4] These biofilms are often resilient and resistant against antibiotics, and constitute one of the major causes for medical device failure.[5] Despite the improvement of aseptic practises, bacterial contamination on medical devices cannot be avoided, given that the human body contains one bacterial cell per each human cell,[6] distributed across the skin, the oral mucosa, and the gastrointestinal track. In this context, the use of intrinsically antimicrobial surfaces provides an important route to tackle the issue at source.

A key strategy to prevent biofilm formation on medical devices is using biocide-releasing antibacterial coatings.[7–9] However, two major innovation challenges need to be considered: First, the modification of medical device materials may encounter strong biocide regulatory barriers, thus requiring strategies that utilise approved chemical agents. Second, there is a need to minimise the impact on existing manufacturing processes and avoid the prohibitive economic costs of replacing mass production facilities. Thus, there is a need to create approaches that may be inserted into the manufacturing processes with minimal impact.

Here, we show that a molecular-level design of operational interfaces can deliver antibacterial function directly at the surface of medical devices. We focus on the design of antimicrobial PDMS surfaces using salicylic acid (SA), a commonly used biocide. PDMS is widely used for manufacturing medical devices, with applications including voice prostheses, [10] venous [11] and urinary catheters.[12] Salicylic acid is approved for use in humans, with a broad mechanism of

action on different bacterial species,[13–15] making it a good candidate for delivering anti-biofilm properties to a PDMS surface.

In this work, we present a rational design to functionalise PDMS surfaces with SA exploiting specific chemical interactions between salicylic acid and amino/imidazoline silane molecules covalently anchored to PDMS. These anchoring moieties are able to promote enhanced loading and release of the biocide from the functional PDMS surfaces. The antimicrobial activity of these surfaces against model Gram-positive and Gram-negative bacteria is demonstrated by a log 6 reduction of planktonic bacterial populations and an efficient anti-biofilm activity at the surface. Importantly, surface-sensitive spectroscopies and density functional theory calculations enable a molecular-level understanding of the interactions that deliver the antibacterial performance.

2. Results and discussion

2.1 Fabrication and characterisation of PDMS surfaces functionalised with salicylic Acid

An effective antibacterial PDMS material must possess the ability to load and release the biocide from its surface and it is, therefore, important that the intermolecular interactions at the functional interface are tailored to deliver this function. Functional PDMS surfaces were fabricated via a generic approach summarised in Figure 1 in which tailored molecules were used as linkers between the PDMS and the SA biocide (see experimental section for details). The linker molecules were chosen to be bifunctional so that they could be directly grafted onto the PDMS using robust covalent chemistry via one end, while inducing softer intermolecular interactions with SA via the other end to enable reversible load-release of the biocide.

A number of functionalised surfaces were created via this step-wise chemical modification, Figure 1. In each case, cured PDMS surfaces were plasma cleaned, prior to functionalisation, to remove organic contaminants at the surface. The impact of each modification step on the interface was evaluated using a combination of ATR-FTIR, Raman and X-ray photoelectron (XPS) spectroscopies.

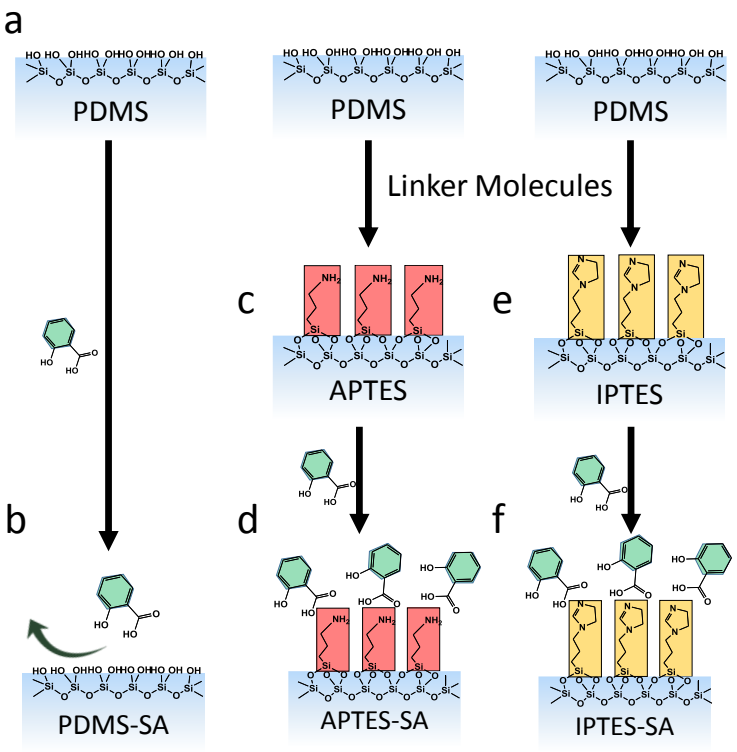

Figure 1. Sequential fabrication of the antibacterial surfaces: (a) PDMS surface (PDMS) (b) exposed to salicylic acid (PDMS-SA); PDMS surface functionalised with (c) APTES linker molecule (APTES) and (d) subsequently loaded with salicylic acid (APTES-SA); PDMS surface functionalised with (e) IPTES linker molecule (IPTES) and (f) subsequently loaded with salicylic acid (IPTES-SA).

A simple approach would be to introduce the SA biocide by directly exposing the molecule to the PDMS surface (Figure 1a and 1b). However, this strategy was unsuccessful with ATR-IR and Raman spectroscopy unable to detect the vibrational bands of SA in the PDMS-SA samples (Figure 2a and 2d). These data suggest that negligible loading of SA is achieved using this approach. We, therefore, created PDMS-Linker-Biocide interfaces, in which linker molecules 3-aminopropyl triethoxysilane (APTES) and 3-(2-Imidazolin-1-yl) propyl triethoxysilane (IPTES)

were incorporated to deliver a dual function at the interfaces. The first function of robust immobilisation onto PDMS was achieved via covalent coupling, exploiting the triethoxysilane functionality to create strong interfacial Si-O bonds. The second function dealt with the efficient loading and release of SA at the interface and was delivered specifically by the amino and the imidazoline functionalities, exploiting their ability to interact with aromatic carboxylic acids via soft H-bonding and π-π interactions. The functionalisation with linker molecules, 3-aminopropyl triethoxysilane (APTES) and 3-(2-Imidazolin-1-yl) propyl triethoxysilane (IPTES) produced the 'APTES' and 'IPTES' surfaces, respectively. These surfaces were subsequently exposed to salicylic acid to yield 'APTES-SA' and 'IPTES-SA' surfaces, as shown schematically in Figure 1.

Both APTES-SA and IPTES-SA samples displayed vibrational signatures associated with salicylic acid, underlining the importance of these linker molecules in loading SA onto the PDMS surface. Distinct IR bands appear at 1486 cm^{-1} and 1456cm^{-1} related to the stretching vibrational modes of the aromatic ring in SA.[16,17], (Figure 2b and 2c). Raman bands attributed to in-plane bending vibrations of the SA phenolic ring at 1143 cm^{-1} and 1032 cm^{-1} were also observed (Figure 2e and 2f). [16,17] The vibrational spectroscopy data also provided insights into the chemical nature of SA at the PDMS interface. Specifically, the absence of the strong carbonyl stretching band between 1650-1700 cm^{-1}, along with the presence of the symmetric stretching of the carboxylate group at 1386 cm^{-1},[18] were consistent with the formation of salicylate species at the interface (Figure 2b and 2c).

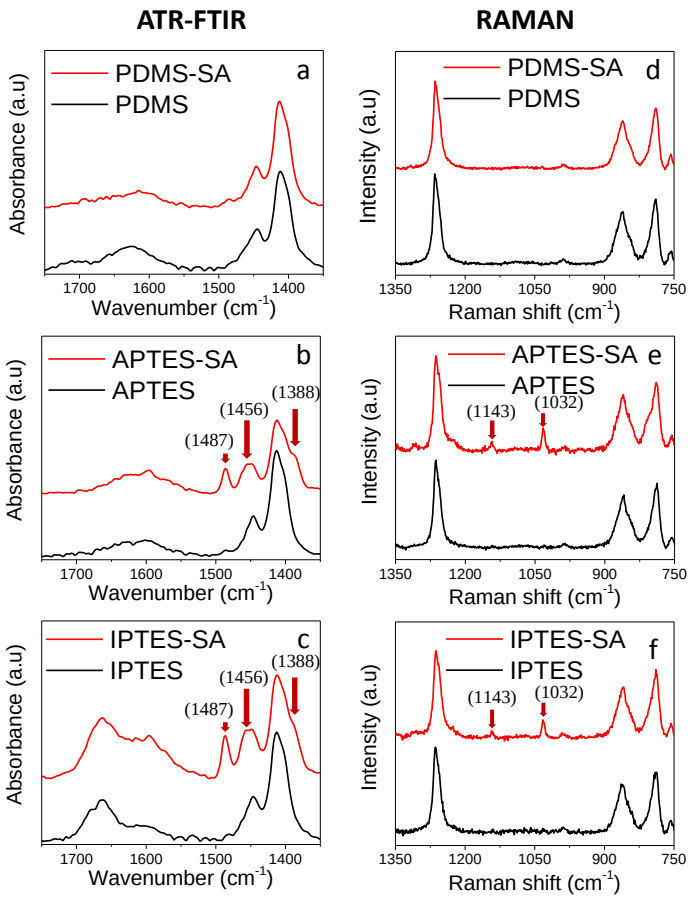

Figure 2. ATR-FTIR (a-c) and Raman (d-f) spectra of PDMS surfaces before and after loading of salicylic acid: (a,c) PDMS and PDMS-SA, (b,d) APTES functionalised PDMS (APTES and APTES-SA), (c,f) imidazoline functionalised PDMS (IPTES and IPTES-SA). Black and red spectra correspond to the substrates before and after salicylic acid functionalisation, respectively. Red arrows show salicylic acid bands observed after loading. Additional spectra for salicylic acid (Figure S1 and Figure S2) and functionalised PDMS surfaces (Figure S3 and Figure S4) can be found in supplementary information.

Spatial distribution of Salicylic Acid across functionalised PDMS surfaces

We investigated the distribution of SA within the PDMS substrate using confocal Raman spectroscopy. The Raman cross-section data revealed a preferential localisation of SA at the interface of APTES and IPTES functionalised PDMS samples (Figure 3, and Figure S5). Distribution along the depth cross-section was monitored exploiting the Raman peak of SA at 1032 cm^{-1}, which lies in a spectral region clear from PDMS peaks. The SA mapping across the PDMS-air interface demonstrated that in the presence of silane functionalisation, SA was loaded ~ 500 microns into the PDMS substrates, showing a rapid decrease in SA concentration as the depth increased. Again, the Raman fingerprint for SA was not observed for the PDMS-SA system, which does not include the silane functionalisation. These experimental results confirmed that the linker silane molecules are key for enhancing the loading capacity of PDMS, creating a reservoir of SA at the interface that can be exploited for controlled release of the biocide.

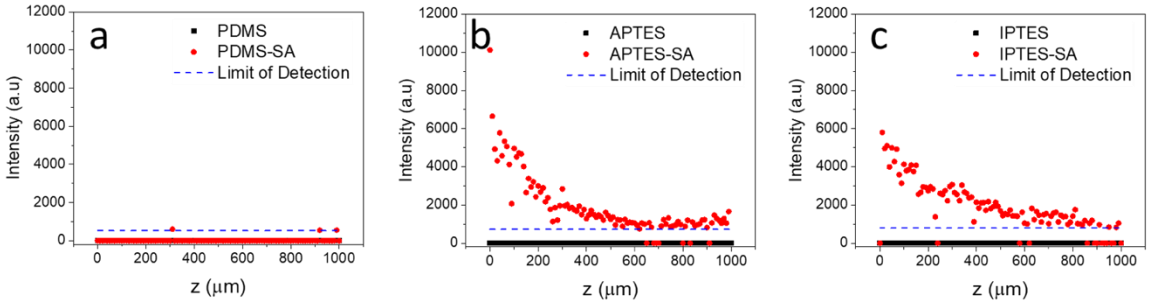

Figure 3. Representative Confocal Raman Spectroscopy cross-section profiles of salicylic acid distribution within different control and silanised surfaces, before and after salicylic acid loading: (a) PDMS and PDMS-SA, (b) APTES and APTES-SA, (c) IPTES and IPTES-SA. Black and red plots correspond to experimental data points from the substrates before and after functionalisation with salicylic acid, respectively. Blue dashed lines indicate experimental detection limit.

2.1 Intermolecular interactions governing the PDMS-Linker-Salicylic Acid interface.

The molecular interactions underpinning the incorporation of SA on APTES and IPTES functionalised surfaces were probed using X-ray Photoelectron Spectroscopy (XPS) and Density Functional Theory (DFT). The N 1s region of the XPS was the most informative since it provided information specifically related to the interface and free from signals arising from the PDMS substrate. Density Functional Theory (DFT) calculations were performed using the M06-2X functional combined with 6-311++G(d,p) basis set, which can accurately describe hydrogen bonding and π-π dispersion forces.[19] We detail below the insights gained for both the APTES-SA and IPTES-SA interfaces.

APTES-SA interfaces

Figure 4a shows the XPS data from the N 1s peaks for the APTES and the APTES-SA interfaces. Essentially, the N 1s peak tracks the behaviour of the APTES molecule since this is the only entity to possess nitrogen atoms within the working interface. The N 1s peak can be deconvoluted into contributions arising from the free amine (~399 eV), the H-bonded NH_2 group (~ 401 eV), and the protonated NH_3^+ group (~402 eV). XPS N 1s data of the APTES samples, Figure 4a, show that up to 62% of nitrogen atoms were present as free amines, with the rest existing as H-bonded and protonated amino groups, attributed to intermolecular NH_2-NH_2 interactions within the APTES layer.[20] Following exposure to SA, this ratio was reversed, with the APTES-SA surfaces displaying 77% of the amines in the protonated form. These results are consistent with the pKa values for APTES and SA (see Table S2).

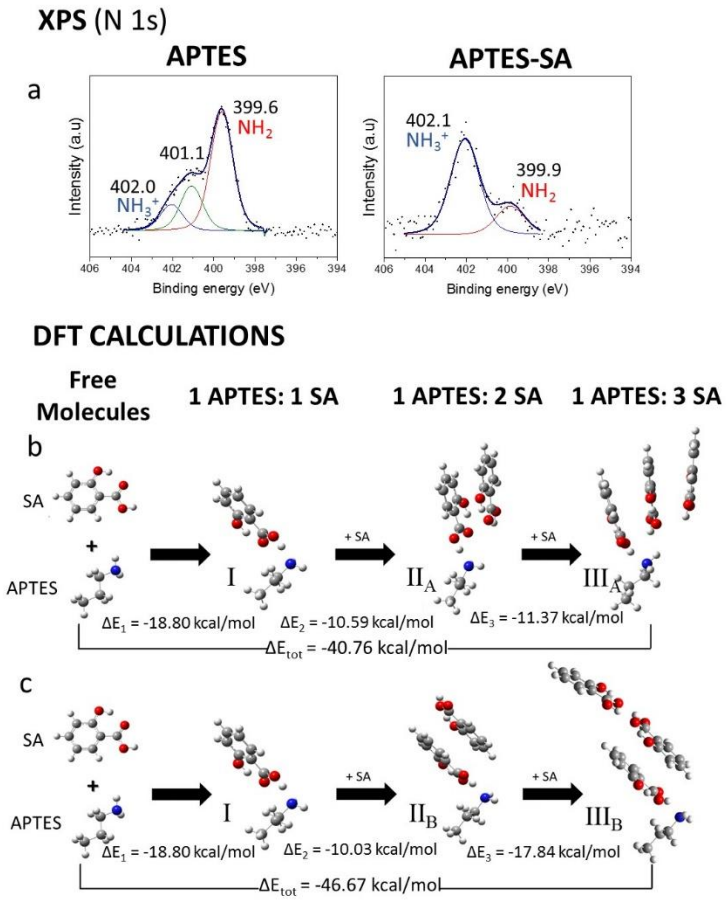

Figure 4. (a) XPS of the N 1s region of APTES and APTES-SA samples, showing an increase in protonated N atoms after functionalisation with salicylic acid (SA). (b,c) DFT calculations of intermolecular interactions occurring at APTES-SA interfaces: APTES-salicylic acid interactions: (I) Strong H-bonding/Proton transfer. Salicylic acid-salicylic acid interactions: (II_A, III_A) Parallel π-π stacking; (II_B) anti-parallel π-π stacking; (III_B) intermolecular hydrogen-bonding. Additional XPS data is presented in SI.

Density Functional Theory (DFT) calculations provide further information into the nature of the SA-APTES interaction. One of the most important insights is that a variety of interactions are energetically favourable and that they can be realised in both 1:1 and 1:n APTES:SA ensembles.

Figure 4 shows the most favourable interactions that arise for 1:1, 1:2 and 1:3 clusters. For the 1:1 dimer, the preferred interaction is via strong proton-sharing between the carboxylic group of salicylic acid and the amino group of APTES, with salicylic acid acting as proton donor, leading to an energy stabilisation of nearly 19 kcal/mol (Interaction I, Figure 4b and 4c). This APTES-SA proton-sharing interaction is significantly stronger than the hydrogen bonding between SA or between water molecules, as indicated by a shorter O···H bond distance and a higher binding energy for the formation of APTES-SA dimer (Table 1).

Table 1. Calculated hydrogen bond energies (E_{HB}), intermolecular O···H bond distance (d_{HB}), and O···H–O bond angle ($\angle_{HB}$) for different molecular dimers (SA: salicylic acid).

Molecular dimer	E_{HB} (kcal/mol)	d_{HB} (Å)	$\angle_{HB}$
water-water*	-5.8	1.99	172.6
SA-SA**	-8.7	1.67	179.1
IPTES-SA	-15.5	1.62	178.7
APTES-SA	-18.8	1.62	168.6

* water dimer data included for comparison [21]
** for SA-SA dimer E_{HB} is normalised, considering two intermolecular hydrogen bonds.

Another important insight from the DFT calculations is that the APTES:SA dimer acts as a nucleation point which enables additional SA molecules to be loaded using a variety of intermolecular SA-SA interactions (Figure S10). For example, in the 1:2 cluster, π-π stacking forces enable parallel (Interaction II_A) and anti-parallel (Interaction II_B) SA-SA stacks to be generated, each bringing an energy stabilisation of ~10 kcal/mol. In the 1:3 ensemble, additional SA molecules can be docked along one direction via further π-π stacking (Interaction III_A) or along the other direction via frontal inter-molecular hydrogen bonding (Interaction III_B), with

significant energy stabilisation of ~11 and ~18 kcal/mol, respectively. The DFT calculations reveal that the chemical structure of the APTES is a key enabler in immobilising the first layer of SA molecules to the PDMS surface, while the inherent chemical structure of SA can exploit a range of intermolecular interactions to create multilayer supramolecular structures[22] with considerable energy stabilisation. The interactions between SA molecules contributed substantially to the stability of the 1:n calculated supramolecular structures shown in Figure 4b-c and, importantly, suggests that several SA molecules can be anchored to one single APTES moiety where, in principle, n could reach high values.

IPTES-SA interfaces

DFT results obtained for the IPTES-SA system display a similar picture (Figure 5b-d and Figure S11). In this case, IPTES is also capable of π-π interactions, adding further complexity to the supramolecular structures. Thus, for the 1:1 dimer structure of IPTES-SA, two distinct configurations can be proposed: (a) frontal hydrogen-bonding with co-planar geometry of SA and IPTES rings (Interaction I_A) or (b) π-π stacking of the IPTES and SA aromatic systems (Interaction I_C). As for the APTES system, the 1:2 and 1:3 families of supramolecular structures can be obtained by adding multiple SA molecules to the 1:1 dimer (Figure 5b-d) and are stabilised by additional energy contributions from π-π interactions (Interaction II_A, II_B, III_A, III_C) or H-bonding (Interaction III_B, II_C), again underlying the role of a single IPTES linker group to nucleate the docking of several salicylic acid molecules.

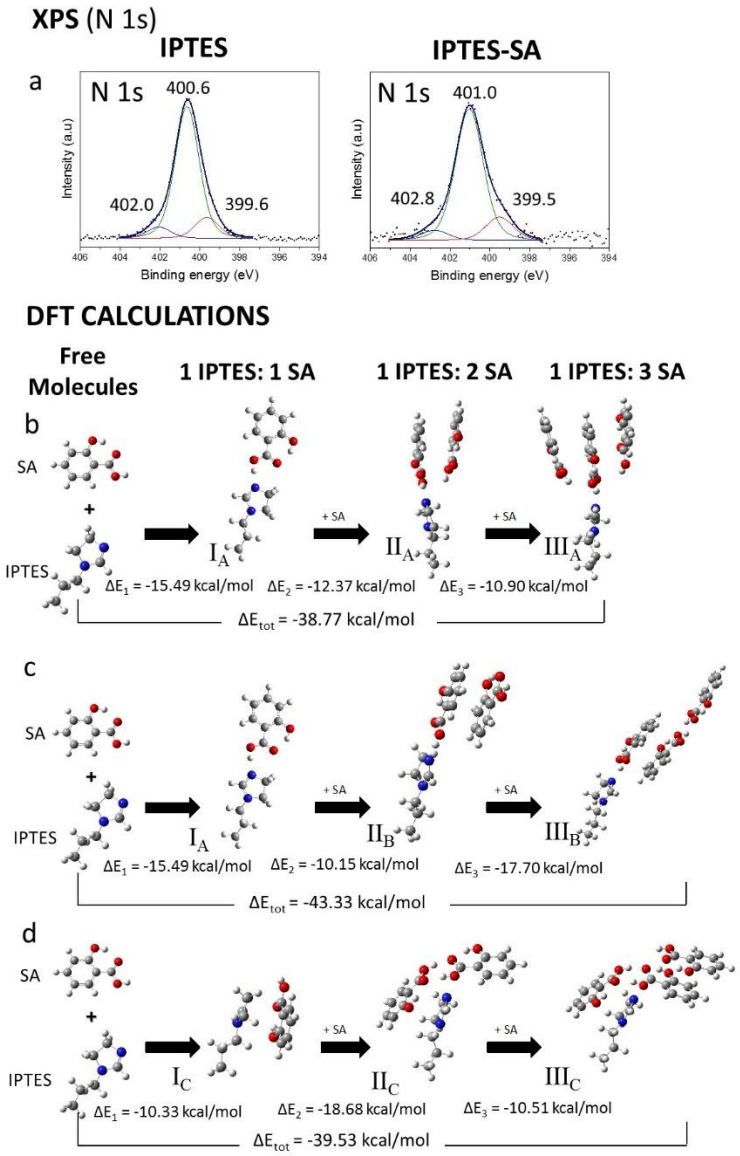

Figure 5. (a) XPS of the N 1s region of IPTES and IPTES-SA samples, showing an increase in protonated N atoms after functionalisation with salicylic acid (SA). (b-d) DFT calculations of intermolecular interactions occurring at IPTES-SA interfaces: IPTES-salicylic acid interactions: (I_A) hydrogen-bonding; (I_C) π-π stacking. Salicylic acid-salicylic acid interactions: (II_A, II_B, III_A, III_C) π-π interactions; (II_C, III_B) hydrogen-bonding. Additional XPS data is presented in SI.

The N1s XPS data for IPTES-SA samples (Figure 5a) show that the N 1s binding energy upshifts from 400.6 to 401 eV upon introduction of the SA and has a value intermediate between that of a free amine (~399 eV) and a protonated amine (~402 eV). This is consistent with the DFT calculations, which show that the IPTES-SA H-bonding is weaker than in APTES-SA, leading to lower energy stabilisation (Table 1).

Our DFT calculations for both APTES-SA and IPTES-SA systems showed that the linker molecules play a pivotal role in docking the first layer of SA molecules to the interface via 1:1 dimers, with an energy stabilisation that can range from ~10 kcal/mol to ~18 kcal/mol. Importantly, these 1:1 dimers promote the docking of further SA molecule at the interface via the formation of a range of complex supramolecular structures in which different bonding modes coexist, creating a local reservoir of SA at the interface.

2.2 Antimicrobial activity of PDMS surfaces functionalised with Salicylic Acid

Release of salicylic acid into aqueous medium

The release of SA from the PDMS surfaces into aqueous medium was evaluated using UV-visible spectroscopy. For this purpose, a model pH buffer based on sodium citrate was optimised to provide optical transparency in the UV region of interest for SA determination, and to resemble the pH response of physiological media typical for biological assays (Figure S12). Under these model buffer conditions, the concentration of SA released after 24h from APTES-SA and IPTES-SA modified PDMS reached 1.46 (± 0.36) mg mL^{-1} and 1.06 (± 0.14) mg mL^{-1}, respectively. PDMS-SA gave a considerably lower SA release of 0.31 (± 0.13) mg mL^{-1} after 24 h, consistent with the significantly reduced loading of SA in these systems. These results also demonstrate that the increased quantities of salicylic acid that can be loaded into silane modified PDMS can be effectively released under physiological conditions.

Effect on planktonic bacteria.

The antimicrobial activity of SA functionalised surfaces against planktonic bacteria was evaluated by measuring the concentration of viable cells in the liquid media in contact with the surfaces, over a period of 24 h. Figure 6 shows the planktonic colony forming unit (CFU) concentrations for three model bacterial species exposed to control and SA modified PDMS surfaces. This data showed that the initial modification of PDMS with either APTES or IPTES silane molecules had no significant effect on the viability of planktonic bacteria, leading to CFU values close to the unmodified PDMS surface. However, for both the APTES-SA and IPTES-SA systems, we observed a drastic reduction of CFU after 24 h of exposure and the plate counting did not reveal viable CFUs. This demonstrates the effectiveness of SA-linker-PDMS interfaces to exert a strong antimicrobial effect on the surrounding environment.

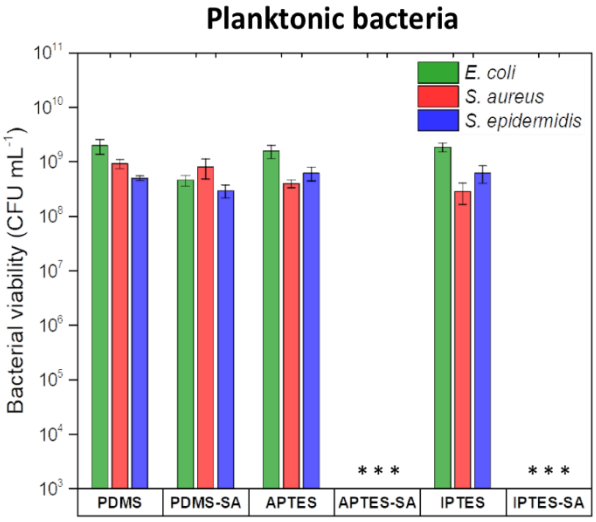

Figure 6. Planktonic viability for *E. coli* (green), *S. aureus* (red), and *S. epidermidis* (blue) after 24 h of incubation onto plasma cleaned PDMS, PDMS surface exposed to salicylic acid (PDMS-SA), APTES functionalised surface (APTES), APTES coated surface loaded with salicylic acid (APTES-SA), IPTES functionalised surface (IPTES) and IPTES coated surface loaded with salicylic acid (IPTES-SA). *Below the detection limit of 1.5×10^2 CFU mL^{-1}.

The observed antimicrobial effect can be directly correlated to the concentration of biocide released from the surfaces as compared to the minimum inhibitory concentration (MIC) and the minimum bactericidal concentration (MBC) of SA against the bacterial strains used (Table 2).

Table 2. Minimum inhibitory concentration (MIC) and Minimum Biocidal Concentration (MBC) for salicylic acid against the bacterial species investigated.

	MIC (mg mL^{-1})	MBC (mg mL^{-1})
E. coli	0.75	0.75
S. aureus	0.56	0.75
S. epidermidis	0.42	0.56

Both the APTES-SA and IPTES-SA systems release a higher concentration of SA than the MIC and the MBC for all three microorganisms, thus delivering a strong antimicrobial effect (>log 6 reduction of CFU respect to a control). In contrast, the release of SA from PDMS-SA is below the MICs and, therefore, there is no significant reduction in the planktonic bacteria compared to the control samples.

We noted that the final pH values for the MBC solutions in the culture media were considerably lower than the starting pH of the growing media, due to the weak-acidic nature of SA. However, the biocidal action of SA cannot be only attributed to the change in pH, since all three bacterial strains were able to grow in nutrient broth solutions acidified with hydrochloric acid to the same pH values (Figure S13). We can, therefore, conclude that, under our experimental conditions, released SA from silane functionalised samples delivered an effective biocidal effect against planktonic cells.

Effect on surface attached bacteria.

Surface-attached bacteria, forming biofilms, tend to be more resistant to the action of biocides.[23,24] We, therefore, also evaluated the viability and density of bacteria directly attached to the PDMS surfaces using confocal laser scanning microscopy (CLSM) and scanning electron microscopy (SEM). Large area, low magnification SEM images show a significant reduction in the number of bacterial cells on APTES-SA and IPTES-SA surfaces, compared to control PDMS and silane functionalised PDMS samples (Figure 7). Live/Dead CLSM imaging enabled the viability of the surface attached cells to be quantitatively evaluated (Figure 8 and Figure 9).

First, we note that the behaviour of the APTES and IPTES surfaces indicate that the presence of the silane linker molecules at the surface has a minor effect on the sessile cells that is species dependent. The number and viability of *S. aureus* is unaffected by either the APTES or the IPTES surfaces. *E. coli* is largely unaffected by the IPTES surface, but the number and viability are slightly compromised the APTES surface. Finally, *S. epidermidis* viability is reduced on both APTES and IPTES surfaces. Molecules containing protonable amines and imidazoline groups have been previously shown to damage bacterial cellular membranes.[25,26] We note, however, the effects of the APTES and IPTES surfaces are relatively small compared to the antimicrobial performance in the presence of the SA functionalisation.

The combined data set shows that when both silane-modified surfaces were loaded with SA, a dramatic reduction in both the density and viability of sessile bacteria is observed (Figure 7-9). Both APTES-SA and IPTES-SA surfaces show a dead fraction of up to ~90% for all three bacterial strains. The biocidal effect shows no distinction between Gram-negative and Gram-positive bacteria, demonstrating a wide spectrum activity. This data, combined with the results

obtained on the experiments for planktonic cells, demonstrates that the PDMS-Linker-SA surfaces display significant antibacterial activity against both planktonic and sessile bacteria.

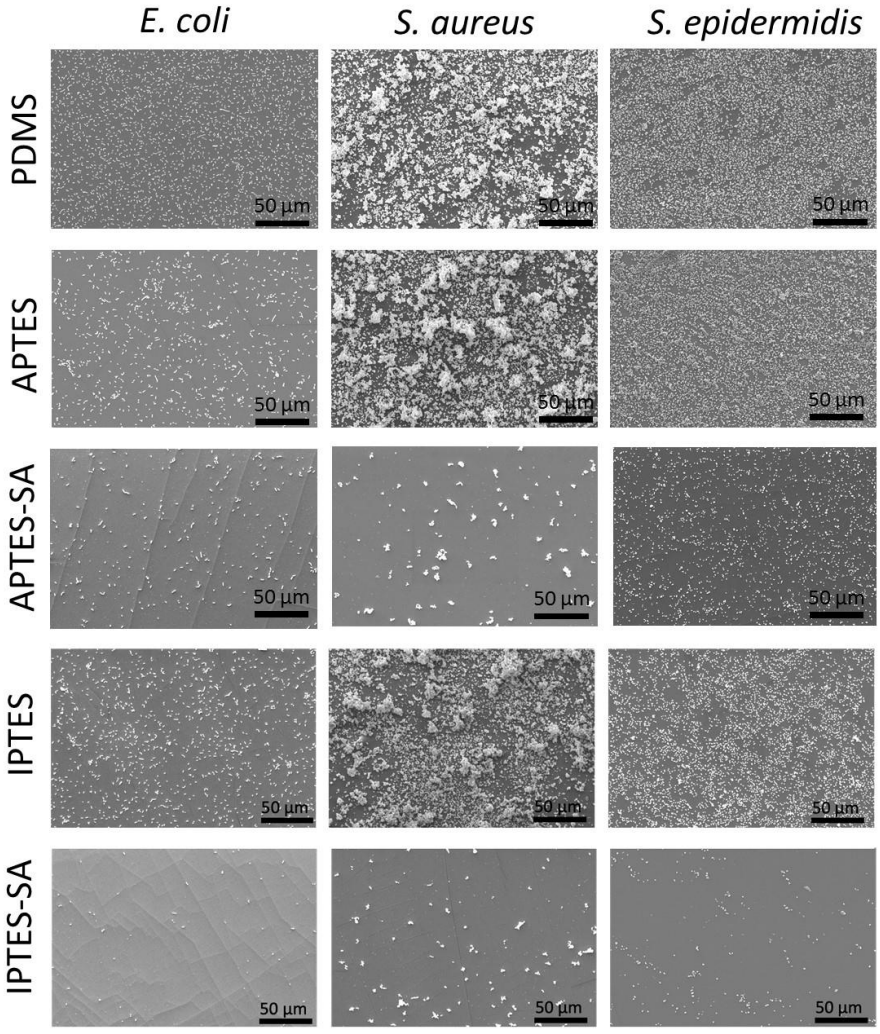

Figure 7. Representative low-magnification (x500) scanning electron microscopy images of surface attached bacteria on PDMS, APTES and IPTES samples with and without SA loading.

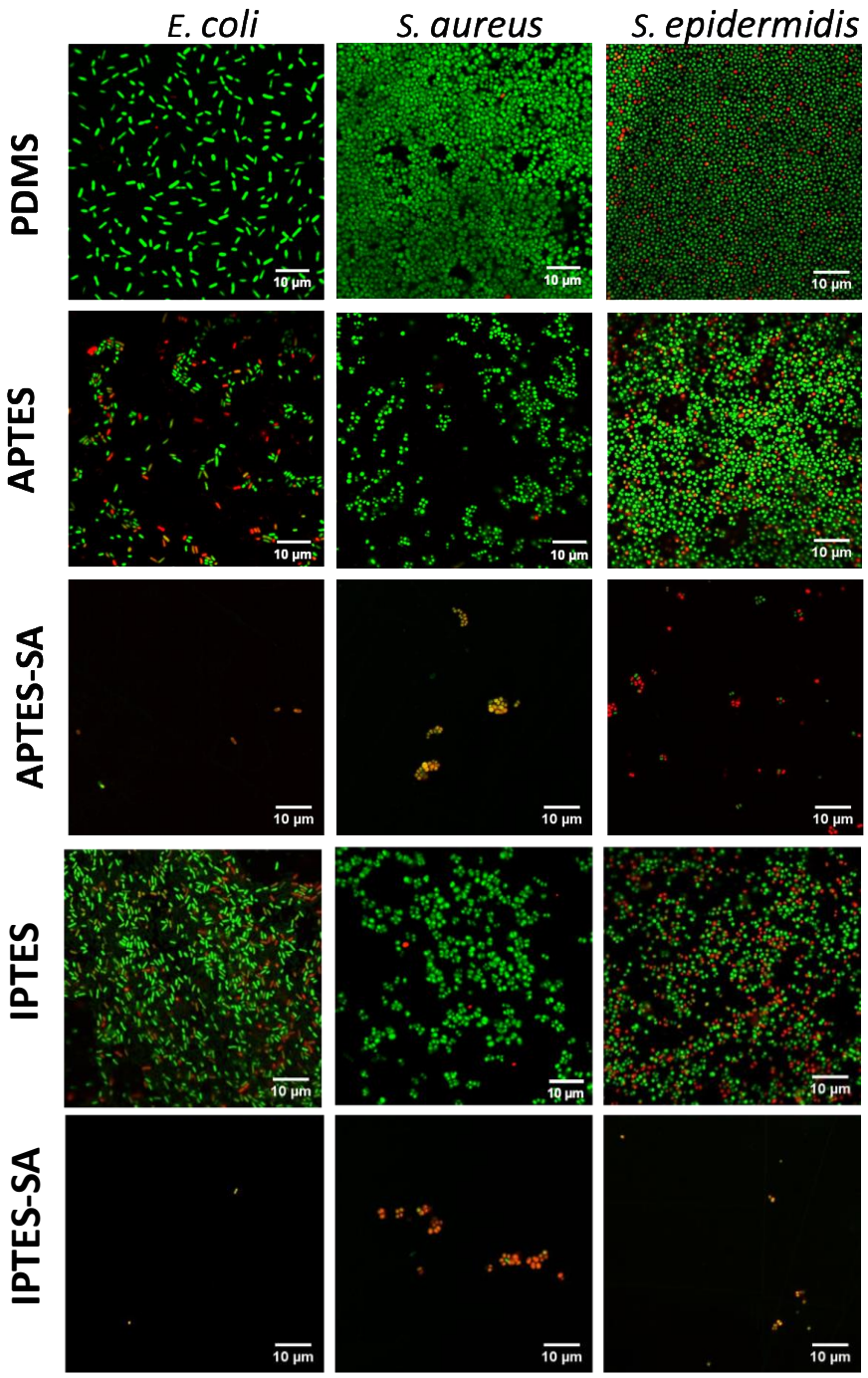

Figure 8. Representative confocal laser scanning microscopy images for live/dead staining with Syto9 (green) and propidium iodide (red) for bacteria attached to PDMS, APTES, APTES-SA, IPTES and IPTES-SA surfaces. By column: *E. coli*, *S. aureus* and *S. epidermidis*.

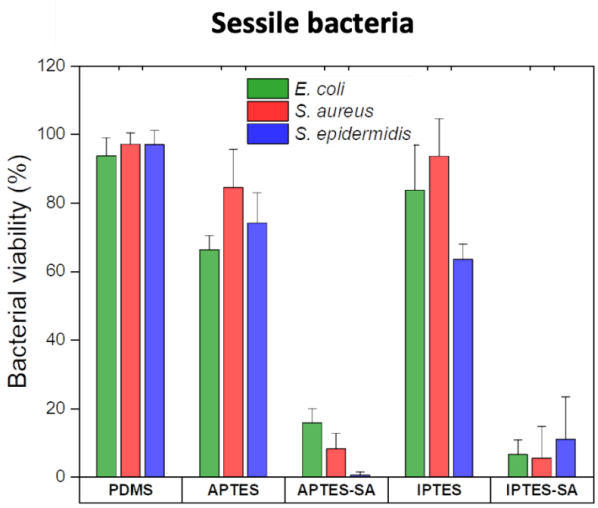

Figure 9. Viability of surface attached *E. coli* (green), *S. aureus* (red), and *S. epidermidis* (blue) after 24 h of incubation on pristine and functionalised PDMS surfaces.

High magnification SEM imaging was used to probe the antimicrobial effect of the surfaces at the single-cell level. Overall, cell morphology seems to remain unaffected by the presence of the silane linkers only at the APTES and IPTES surfaces in the absence of SA. However, this situation changes drastically when SA is introduced to the interface, with the morphology of the bacterial cell envelopes being heavily compromised on APTES-SA and IPTES-SA surfaces (Figure 10 and Figure S14). For example, the rod-shaped *E. coli* cells display a loss of their integrity predominantly at the polar ends. For *S. aureus* and *S. epidermidis*, there is loss of spherical symmetry, with considerable increase of roughness and/or collapse of the cell wall. These results suggest that the mode of action of SA involves destabilisation of the membrane integrity and subsequent disruption of cell envelope, as previously reported.[27] These results were systematically observed for both APTES-SA and IPTES-SA surfaces, confirming that the two silane functionalities act as effective interfacial dockers and carriers for the biocide, which upon release compromises the viability of colonising bacteria. The remarkable reduction of the

number and viability of sessile bacteria demonstrates that the surfaces developed herein are effective for prevention of bacterial biofilms.

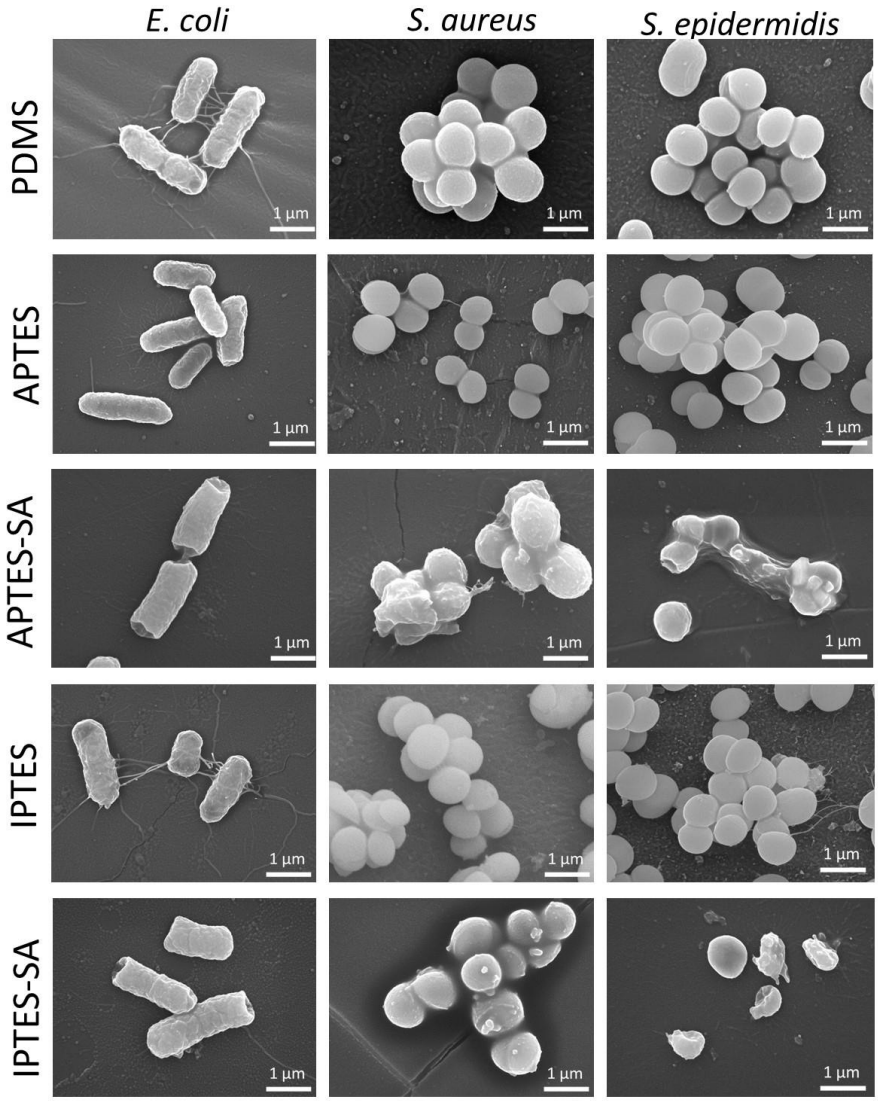

Figure 10. Representative high-magnification (x20,000) scanning electron microscopy images of surface attached bacteria on pristine PDMS, APTES, APTES salicylic acid (APTES-SA) functionalised, IPTES and IPTES salicylic acid (IPTES-SA) functionalised PDMS surfaces.

3. Conclusion

Antibacterial PDMS surfaces were created via a generic strategy that exploited bi-functional silane linker molecules to create PDMS-Linker-Biocide interfaces. Specifically, the triethoxysilane functionality was used to graft one end of the linker onto the PDMS via the creation of strong covalent Si-O bonds, while the other end displayed amino or imidazoline functionalities to dock salicylic acid molecules via soft H-bonding and π-π interactions. The molecular interactions within this three-component interface were investigated by complementary spectroscopic techniques (FTIR, Raman and X-ray Photoelectron Spectroscopies) and DFT calculations. These data show that the uptake of SA at the interface occurs via two steps. First, each linker molecule attracts a single SA molecule to create a 1:1 linker:SA dimer held together by soft interactions and providing significant energy stabilisation. Subsequently, each 1:1 complex provides a nucleation point that attracts further biocide molecules via the stabilisation of supramolecular SA structures held together by H-bonding and π–π stacking interactions. This enables a single linker molecule to attract multiple SA molecules, thus significantly enhancing biocide uptake at the interface. Importantly, the use of soft H-bonding and π–π interactions to create a reservoir of SA molecules at the PDMS surface is also important in delivering the ability to subsequently release the SA into the environment or to attached bacterial species in order to deliver the antimicrobial effect.

Antibacterial properties of the modified PDMS surfaces were tested against sessile and planktonic *E. coli, S. aureus* and *S. epidermidis* cells. Both APTES-SA and IPTES-SA surfaces reduced the number of viable bacteria in the planktonic state to values under the detection limit for the CFU assay. The viability and morphology of persistent sessile bacteria were assessed using Live/dead staining, laser scanning microscopy and scanning electron microscopy. These

data showed that the density of sessile bacterial cells was considerably reduced on APTES-SA and IPTES-SA surfaces and that the morphology of the attached bacteria was heavily compromised leading to a dead fraction of up to 90%. The biocidal effect was present for both Gram-negative and Gram-positive bacteria, demonstrating a wide spectrum activity. Finally, the simple two-step functionalisation approach is easily translated to the manufacture of antimicrobial medical devices to prevent surface colonisation and systemic infections by Gram-positive and Gram-negative bacteria.

4. Experimental Section

Synthesis and chemical characterisation of PDMS surfaces

Fabrication of PDMS substrates: PDMS (Sylgard 184 silicone elastomer kit, Dow Corning) was mixed at 10:1 base to curing agent ratio. The two components were thoroughly mixed and degassed under vacuum for 25 min to remove trapped air bubbles. The mixture was poured into individual wells of 24-well plates and heat-cured at 70 $^{\circ}$C for 5 h. The surface area of each PDMS substrate was determined by the diameter of each individual well (~ 188 mm^2), while the thickness (~19.4 ± 0.31 mm) was reproduced within a 15% of deviation.

Functionalisation of PDMS surfaces: PDMS substrates underwent a two-step surface modification process, which resulted in six different surface types. First, all PDMS surfaces were cleaned using a Zepto plasma cleaning system (Diener Electronic GmBH) applying 20 W radiofrequency power at 40 kHz for 1 min at 0.3 mbar constant air pressure. This step also ensured the presence of reactive SiO_2 at the surface of PDMS,[28] enabling further functionalisation with silane molecules. PDMS-linker surfaces were created by immersion in 10% (v/v) ethanolic solutions of (3-aminopropyl) triethoxysilane (APTES, Fluorochem) or 3-(2-Imidazolin-1-yl) propyl triethoxysilane (IPTES, Fluorochem) for 2 h at 50 °C. Samples were rinsed three times with ethanol to remove physisorbed silane molecules and dried at room temperature. The silanisation process was used to fabricate APTES and IPTES surfaces, by introducing amine and imidazoline functional groups at the surface, respectively. Assuming a complete monolayer of silane molecules,[29] we estimated a surface coverage of at least 2×10^{14} molecules/cm^2. Subsequently, PDMS, APTES and IPTES were immersed for 20 h in a 200 mM salicylic acid solution in 50/50 ethanol/water, and repeatedly washed with DI water and ethanol

to obtain PDMS-SA, APTES-SA and IPTES-SA surfaces, respectively. Details of the chemical compounds used for surface functionalisation are included in Table S2.

Chemical Characterisation of PDMS surfaces: Pristine and modified PDMS surfaces were investigated by attenuated total reflectance – Fourier transform infrared (ATR-FTIR), X-ray photoelectron spectroscopy (XPS) and Raman spectroscopy. Infrared measurements were performed using a Bruker Alpha FT-IR with Platinum ATR module with a resolution of $4cm^{-1}$. Each spectrum was the average of 24 scans. Sample spectra were collected in the 400-4000 cm^{-1} range and analysed using OPUS Spectroscopy Software (Bruker).

The surface Raman spectra were recorded with a Renishaw inVia Confocal Raman microscope using an excitation wavelength of 532 nm at 50% power and a 20x objective lens, with 8 seconds acquisition time. Raman spectra were processed using WiRE 4.4 software (Renishaw).

XPS data of pristine and modified PDMS surfaces were recorded on a Kratos Axis Supra instrument using monochromatic Al Kα radiation (1486.7 eV, 150 W). Survey scan spectra were acquired using a pass energy of 160 eV and a 1 eV step size. Narrow region scans of C 1s and N 1s were acquired using a pass energy of 20 eV and a 0.1 eV step size. A charge neutraliser was used to compensate the electrically insulating nature of the samples. The spectra were calibrated post acquisition to the binding energy of 285.0 eV for the hydrocarbon C 1s peak. Data was processed and analysed using CasaXPS and Kratos ESCApe software (Kratos).

Raman spectroscopy of PDMS cross-sections: Modified PDMS substrates were cut transversally and the cross-sections of the samples were spectroscopically examined using a Renishaw inVia Confocal Raman microscope. The Raman spectra of the modified PDMS samples were obtained using a map image acquisition mode, sampling every 10 μm starting from the top of the surface (x_o=0 μm) to a distance equivalent to 1 mm within the material (x_f=1000

μm). For each measurement, an excitation wavelength of 532 nm and a 50% power were selected, using a 20x Leica objective lens and 8 seconds acquisition time. The Wire 4.4 analysis software (Renishaw) allowed correction of the baseline for each individual spectrum. The distribution of salicylic acid through the sample cross-section was monitored measuring the intensity of the Raman band at 1032 cm^{-1}. The intensity of the band at 1032 cm^{-1} was obtained by determining the baseline corrected peak intensity from 1020 to 1045 cm^{-1}. Cross-section data points below the experimental detection limit were set to zero.

Salicylic acid release from modified PDMS: The release of salicylic acid from PDMS-SA, APTES-SA and IPTES-SA surfaces was evaluated by UV-VIS spectrophotometry measuring the absorbance at 299 nm. The volume/surface ratio and the temperature were adjusted to reproduce the conditions of the biological assays, using 750 μL of pH 7 citrate model buffer and incubating the samples for 24 h at 37 ^{o}C. The citrate model buffer replaced the nutrient broth (NB) used in the bacterial viability experiments, since NB is not transparent in the UV-VIS region of interest. The model buffer was prepared by dissolving specific amounts of sodium citrate (Sigma Aldrich) and citric acid (Sigma Aldrich) in DI water to produce a pH 4.8 10 mM citrate buffer solution. The final pH of this model buffer was adjusted to pH 7 using a 1 M sodium hydroxide solution (Sigma Aldrich).

Theoretical Methods

Density functional theory calculations: Density functional theory (DFT) calculations were performed with the Gaussian 09 program[30] using M06-2X functional combined with 6-311++G(d,p) basis set. Geometry optimisations were performed until forces and displacements were below reasonable thresholds and frequency calculations were performed to ensure minima. Interaction energies were computed using the following equation

$$E_{\text{int}} = E_{Mol1+Mol2} - E_{Mol1} - E_{Mol2}$$

Where Mol1 and Mol2 are the individual components and Mol1+Mol2 represents the complex or dimeric structure. For example, in the APTES-SA system, Mol1 is the amino group of APTES and Mol2 is the salicylic acid (SA) molecule, and Mol1+Mol2 is the dimer APTES-SA. In cases where multiple salicylic acid molecules were considered, Mol1+Mol2 was the APTES/IPTES-(n+1)SA complex, Mol1 was the salicylic acid molecule and Mol2 was the APTES/IPTES-(n)SA complex; this enabled us to evaluate the individual contribution of each additional salicylic acid and, therefore, the potential for multi-stacking of salicylic acid molecules. Evaluation of the potential energy landscape for π- π stacked SA-SA and IPTES-SA dimers was performed imposing constrains to selected dihedrals (composed of two atoms from each ring) and scanning the full angular range (0-360º). Geometry optimisations were performed for each point in the dihedral scans and the lowest energy configurations were selected for unconstrained geometry optimizations. Further selections of initial conformations were based on chemical intuition, testing a large number of viable conformations, and reporting lowest energy geometries.

Antibacterial performance of modified PDMS surfaces

Viability of planktonic bacteria: *Escherichia coli* (ATCC 10798), *Staphylococcus aureus* (DSM 346) and *Staphylococcus epidermidis* (ATCC 12228) were transferred from the stock to a fresh agar plate and incubated overnight at 37 °C. Three colonies of each species were taken from the agar plate, transferred to fresh nutrient broth (NB) medium (Oxoid, Ltd-Thermo Fisher) and grown overnight in a shaking incubator (200 rpm, at 37 °C). The bacterial cell concentration was adjusted to 10^5 colony forming units per millilitre (CFU mL^{-1}) in sterile NB for each of the bacterial strains. Modified PDMS surfaces were sterilised with UV light for 20 min and placed in a sterile 24-well plate. Then, 750 µL of 10^5 CFU mL^{-1} bacterial suspension in NB were added to

each of the wells and the plates were incubated for 24 h at 37 °C. At the end of each incubation period, serial dilutions of the resulting suspensions were performed to determine the planktonic bacterial viability by CFU mL^{-1} counting. Viability assays of planktonic bacteria were performed in triplicate.

Determination of Minimum Inhibitory Concentration (MIC) and Minimum Bactericidal Concentration (MBC): *E. coli* (ATCC 10798), *S. aureus* (DSM 346) and *S. epidermidis* (ATCC 12228) were grown as stated above. Bacterial cell concentration was adjusted to 10^5 CFU mL^{-1} in sterile NB for each bacterial strain. Then, 100 µL of the bacterial solution were added to the microwells of a sterile 96-well plate containing 100 µL of salicylic acid solutions at different concentrations. The plates were placed in a FilterMax F5 Multimode Plate Reader (Molecular Devices) and the optical density at 595 nm was screened every 30 min for 24 h at 37°C. The MIC was calculated as the minimum salicylic acid concentration that prevented a detectable optical density increase. After incubation, the bacterial solutions from the non-growing microwells were taken and diluted in fresh NB (2-fold dilution). 20 µL from each solution were transferred to a fresh agar plate and incubated for 48 h. The MBC was calculated as the minimum concentration that did not show bacterial colonies on the agar plate.

Viability of sessile bacteria: The viability and the density of bacteria attached to the surfaces were investigated by fluorescence microscopy and scanning electron microscopy (SEM). In both cases, *E. coli*, *S. aureus* and *S. epidermidis* were incubated over pristine or modified PDMS surfaces for 24 h, as described in the previous section. For each bacterium, experiments were carried out as three independent biological replicates.

Prior to confocal fluorescence imaging, functionalised PDMS surfaces were washed 3 times with sterile 0.85% (w/w) NaCl solution and stained with Live/dead BacLight Bacterial Viability kit (Molecular Probes, L7012). In this test, 1 mL of a sterile 0.85% solution containing mixtures of SYTO 9 (green-fluorescent nucleic acid stain for all cells), and propidium iodide (red-fluorescent nucleic acid stain for dead cells) was added to each sample in a 24-well plate and incubated for 15 min in the dark at room temperature. After staining, the surfaces were immediately imaged using a confocal upright Zeiss LSM 880 Multiphoton microscope. Images were analysed with an in-house script based on Fiji software.

SEM samples were incubated for 24 h with bacteria and fixed overnight at 4 °C with 4% paraformaldehyde and 2.5% glutaraldehyde in 0.1 M phosphate buffer. Sample fixation was completed in four sequential steps using 2% osmium tetroxide, 1% tannic acid, 2% osmium tetroxide and 1% uranyl acetate solutions in water. Every step was assisted by a Biowave Pro Microwave system (Pelco). For each step, samples were exposed to cycles of 100W microwave radiation for 20 s and subsequently cooled down for 20 s. This process was repeated three times per microwaving step. Between each staining step, the samples were thoroughly rinsed with DI-water. After the final uranyl acetate staining, the samples were rinsed with DI-water, and progressively dehydrated with different volumetric ratios of ethanol (i.e. 30%, 50%, 70%, 80%, 90% and 100%). After dehydration, modified and control PDMS samples were critical-point dried in CO_2 (Quorum Technologies K850) and sputter coated with 10 nm of Au/Pd (Quorum Technologies Q150T) for SEM imaging at 10 kV using a JEOL SEM 7001 system.

Supporting Information

SI contains additional spectroscopic data on pure salicylic acid and on functionalised surface, DFT calculations for the π-π stacked systems, details on the model buffer, biological response at acidic pH, and additional SEM images of sessile bacteria.

Acknowledgements

We would like to thank David Mason and Marco Marcello from the Liverpool Centre for Cell Imaging (CCI) for help with experimental design and image analysis support. We also acknowledge the support of University of Liverpool Biomedical Electron Microscopy Unit and Imaging Centre at Liverpool (ICAL).We acknowledge the Centre for High Performance Computing, Cape Town, South Africa for computational resources to run the Gaussian calculations. This work was partly funded by EPSRC (grant number EP/N51004X/1) and Innovate UK (project reference 101489, TS/L001985/1). This work was also supported by funding from the Biotechnology and Biological Sciences Research Council (Award Number BB/R012415/1). ISB, YDF and FM are funded by the National Biofilms Innovation Centre (NBIC) which is an Innovation and Knowledge Centre funded by the Biotechnology and Biological Sciences Research Council, Innovate UK and Hartree Centre.

References

(1) Bryers, J. D. Medical Biofilms. *Biotechnol. Bioeng.* **2008**, *100* (1), 1–18. https://doi.org/10.1002/bit.21838.

(2) Friedrich, A. W. Control of Hospital Acquired Infections and Antimicrobial Resistance in Europe: The Way to Go. *Wiener Medizinische Wochenschrift* **2019**, *169* (S1), 25–30. https://doi.org/10.1007/s10354-018-0676-5.

(3) Characklis, W. G.; Marshall, K. C. *Biofilms*; Wiley: New York, 1990.

(4) Garrett, T., Bhakoo, M., y Zhang, Z. Bacterial Adhesion and Biofilms on Surfaces. *Prog. Nat. Sci.* **2008**, *18* (9), 1049–1056. https://doi.org/http://dx.doi.org/10.1016/j.pnsc.2008.04.001.

(5) Buhmann, M. T.; Stiefel, P.; Maniura-Weber, K.; Ren, Q. In Vitro Biofilm Models for Device-Related Infections. *Trends in Biotechnology*. 2016, pp 945–948. https://doi.org/10.1016/j.tibtech.2016.05.016.

(6) Bianconi, E.; Piovesan, A.; Facchin, F.; Beraudi, A.; Casadei, R.; Frabetti, F.; Vitale, L.; Pelleri, M. C.; Tassani, S.; Piva, F., Perez-Amodio S.; Strippoli P.; Canaider S.; An Estimation of the Number of Cells in the Human Body. *Ann. Hum. Biol.* **2013**, *40* (6), 463–471. https://doi.org/10.3109/03014460.2013.807878.

(7) Koo, H.; Allan, R. N.; Howlin, R. P.; Stoodley, P.; Hall-Stoodley, L. Targeting Microbial Biofilms: Current and Prospective Therapeutic Strategies. *Nat. Rev. Microbiol.* **2017**, *15* (12), 740–755. https://doi.org/10.1038/nrmicro.2017.99.

(8) Nowatzki, P. J.; Koepsel, R. R.; Stoodley, P.; Min, K.; Harper, A.; Murata, H.; Donfack, J.; Hortelano, E. R.; Ehrlich, G. D.; Russell, A. J. Salicylic Acid-Releasing Polyurethane

Acrylate Polymers as Anti-Biofilm Urological Catheter Coatings. *Acta Biomater.* **2012**, *8* (5), 1869–1880. https://doi.org/10.1016/j.actbio.2012.01.032.

(9) Wang, B.; Liu, H.; Wang, Z.; Shi, S.; Nan, K.; Xu, Q.; Ye, Z.; Chen, H. A Self-Defensive Antibacterial Coating Acting through the Bacteria-Triggered Release of a Hydrophobic Antibiotic from Layer-by-Layer Films. *J. Mater. Chem. B* **2017**, *5* (7), 1498–1506. https://doi.org/10.1039/c6tb02614a.

(10) Ferreira, P.; Carvalho, Á.; Correia, T. R.; Antunes, B. P.; Correia, I. J.; Alves, P. Functionalization of Polydimethylsiloxane Membranes to Be Used in the Production of Voice Prostheses. *Sci. Technol. Adv. Mater.* **2013**, *14* (5), 55006. https://doi.org/10.1088/1468-6996/14/5/055006.

(11) Chauhan, A.; Bernardin, A.; Mussard, W.; Kriegel, I.; Estève, M.; Ghigo, J. M.; Beloin, C.; Semetey, V. Preventing Biofilm Formation and Associated Occlusion by Biomimetic Glycocalyxlike Polymer in Central Venous Catheters. *J. Infect. Dis.* **2014**, *210* (9), 1347–1356. https://doi.org/10.1093/infdis/jiu249.

(12) Singha, P.; Locklin, J.; Handa, H. A Review of the Recent Advances in Antimicrobial Coatings for Urinary Catheters. *Acta Biomater.* **2017**, *50*, 20–40. https://doi.org/10.1016/J.ACTBIO.2016.11.070.

(13) Price, C. T. D.; Lee, I. R.; Gustafson, J. E. The Effects of Salicylate on Bacteria. *Int. J. Biochem. Cell Biol.* **2000**, *32* (10), 1029–1043. https://doi.org/10.1016/S1357-2725(00)00042-X.

(14) Farber, B. F.; Teichberg, S.; Wolff, A. G.; Roberts, B. Salicylic Acid Decreases Extracellular Biofilm Production by Staphylococcus Epidermidis: Electron Microscopic Analysis. *J. Infect. Dis.* **1993**, *167* (6), 1501–1503. https://doi.org/10.1093/infdis/167.6.1501.

(15) Perilli, R.; Marziano, M. L.; Formisano, G.; Caiazza, S.; Scorcia, G.; Baldassarri, L. Alteration of Organized Structure of Biofilm Formed by Staphylococcus Epidermidis on Soft Contact Lenses. *J. Biomed. Mater. Res.* **2000**, *49* (1), 53–57. https://doi.org/10.1002/(SICI)1097-4636(200001)49:1<53::AID-JBM7>3.0.CO;2-C.

(16) Humbert, B.; Alnot, M.; Quilès, F. Infrared and Raman Spectroscopical Studies of Salicylic and Salicylate Derivatives in Aqueous Solution. *Spectrochim. Acta - Part A Mol. Biomol. Spectrosc.* **1998**, *54* (3), 465–476. https://doi.org/10.1016/S1386-1425(97)00239-4.

(17) Philip, D.; John, A.; Panicker, C. Y.; Varghese, H. T. FT-Raman, FT-IR and Surface Enhanced Raman Scattering Spectra of Sodium Salicylate. *Spectrochim. Acta - Part A Mol. Biomol. Spectrosc.* **2001**, *57* (8), 1561–1566. https://doi.org/10.1016/S1386-1425(01)00395-X.

(18) Alvarez-Ros, M. C.; Sánchez-Cortés, S.; García-Ramos, J. V. Vibrational Study of the Salicylate Interaction with Metallic Ions and Surfaces. *Spectrochim. Acta - Part A Mol. Biomol. Spectrosc.* **2000**, *56* (12), 2471–2477. https://doi.org/10.1016/S1386-1425(00)00328-0.

(19) Walker, M.; Harvey, A. J. A.; Sen, A.; Dessent, C. E. H. Performance of M06, M06-2X, and M06-HF Density Functionals for Conformationally Flexible Anionic Clusters: M06 Functionals Perform Better than B3LYP for a Model System with Dispersion and Ionic Hydrogen-Bonding Interactions. *J. Phys. Chem. A* **2013**, *117* (47), 12590–12600. https://doi.org/10.1021/jp408166m.

(20) Zhang, F.; Srinivasan, M. P. Self-Assembled Molecular Films of Aminosilanes and Their Immobilization Capacities. *Langmuir* **2004**, *20* (6), 2309–2314. https://doi.org/10.1021/la0354638.

(21) Pal, S.; Kundu, T. K. Theoretical Study of Hydrogen Bond Formation in Trimethylene Glycol-Water Complex. *ISRN Phys. Chem.* **2012**, *2012*, 1–12. https://doi.org/10.5402/2012/570394.

(22) Montis, R.; Hursthouse, M. B. Surprisingly Complex Supramolecular Behaviour in the Crystal Structures of a Family of Mono-Substituted Salicylic Acids. *CrystEngComm* **2012**, *14* (16), 5242–5254. https://doi.org/10.1039/c2ce25336d.

(23) Luppens, S. B. I.; Reij, M. W.; van der Heijden, R. W. L.; Rombouts, F. M.; Abee, T. Development of a Standard Test To Assess the Resistance of Staphylococcus Aureus Biofilm Cells to Disinfectants. *Appl. Environ. Microbiol.* **2002**, *68* (9), 4194–4200. https://doi.org/10.1128/AEM.68.9.4194-4200.2002.

(24) Stewart, P. S.; Costerton, J. W. Antibiotic Resistance of Bacteria in Biofilms. *Lancet* **2001**, *358* (9276), 135–138. https://doi.org/10.1016/S0140-6736(01)05321-1.

(25) Salem, A. M.; Adams, D.; Newman, H. N.; Rawle, L. W. Antimicrobial Properties of 2 Aliphatic Amines and Chlorhexidine in Vitro and in Saliva. *J. Clin. Periodontol.* **1987**, *14* (1), 44–47. https://doi.org/10.1111/j.1600-051X.1987.tb01512.x.

(26) Harris, K. K.; Fay, A.; Yan, H. G.; Kunwar, P.; Socci, N. D.; Pottabathini, N.; Juventhala, R. R.; Djaballah, H.; Glickman, M. S. Novel Imidazoline Antimicrobial Scaffold That Inhibits

DNA Replication with Activity against Mycobacteria and Drug Resistant Gram-Positive Cocci. *ACS Chem. Biol.* **2014**, *9* (11), 2572–2583. https://doi.org/10.1021/cb500573z.

(27) Monte, J.; Abreu, A.; Borges, A.; Simões, L.; Simões, M. Antimicrobial Activity of Selected Phytochemicals against Escherichia Coli and Staphylococcus Aureus and Their Biofilms. *Pathogens* **2014**, *3* (2), 473–498. https://doi.org/10.3390/pathogens3020473.

(28) Befahy, S.; Lipnik, P.; Pardoen, T.; Nascimiento C.; Patris B.; Bertrand, P.; Yunus S. Thickness and Elastic Modulus of Plasma Treated PDMS Silica-like Surface Layer. *Langmuir* **2010**, 26 (5), 3372–3375 https://doi.org/10.1021/la903154y

(29) Pallavicini, P.; Dacarro, G.; Diaz-Fernandez, Y. A.; Taglietti A. Coordination chemistry of surface-grafted ligands for antibacterial materials. *Coord. Chem. Rev.,* **2014**, 275, 37-53 https://doi.org/10.1016/j.ccr.2014.04.013

(30) Frisch, M. J.; Trucks, G. W.; Schlegel, H. B.; Scuseria, G. E.; Robb, M. A.; Cheeseman, J. R.; Scalmani, G.; Barone, V.; Petersson, G. A.; Nakatsuji, H.; Li X.; Caricato M.; Marenich A.; Fox D. J. Gaussian 09, Revision E.01. 2013, Gaussian, Inc., Wallingford CT, **2016**.